A Quasi-Lagrangian Regional Model Designed for Operational Weather Prediction

MUKUT B. MATHUR

National Meteorological Center, Washington, DC 20233

(Manuscript received 26 March 1983, in final form 18 July 1983)

ABSTRACT

A regional numerical weather prediction model is designed using the quasi-Lagrangian method for operational forecasting of synoptic and mesoscale disturbances. The nonlinear advective terms and the total forcing experienced by a fluid parcel are evaluated with high order accuracy. Many physical processes such as convective and nonconvective release of latent heat are incorporated.

The model can be integrated over any geographical area, with any horizontal and vertical resolution, and with either a uniform grid or two nested grids.

Results are presented for 48 h forecasts produced by the model utilizing operational limited area analyses. Lateral boundary values were obtained from a previous run of the operational large-scale model. The model's predictions are compared to those obtained using the National Meteorological Center's currently operational regional model.

1. Introduction

The limited area fine mesh (LFM) model (Gerrity, 1977; Deaven, 1982) is used at the National Meteorological Center (NMC) for operational prediction over North America. Features of the atmospheric large-scale circulation and precipitation are predicted reasonably well by the LFM model, but it is generally recognized that significant improvements can be achieved only by increasing the model's resolution and by improving its parameterization of the subgrid physical processes. The horizontal and vertical resolution of the LFM model is fixed. Additionally, the design of the LFM model is such that it is a formidable task to incorporate new physical parameterization procedures.

A quasi-Lagrangian nested grid model (QNGM) was recently developed at NMC. It was designed for operational prediction of mesoscale and synoptic-scale disturbances. The model can be integrated over any limited geographical area, and with any horizontal and vertical resolution. Two versions of the model were developed: one uses a uniform horizontal resolution, the other uses two nested grids. The nesting procedure allows for two-way interaction of the solutions between the fine and coarse grids. The procedure is the same as used in a previous work (Mathur, 1974).

Another important feature of QNGM is that it is modular. Physical parameterization may be varied without significant restructuring of the code. The code is well suited for comparative studies of the effects produced by different parameterization procedures.

A one-step, second-order, quasi-Lagrangian scheme is used to integrate the model. A special feature of this scheme is that it accounts for changes in accelerations of dependent variables and advecting velocity over the trajectory traced by the parcel in time step Δt. The inclusion of this formulation of the advective process should give accurate prediction of the phase and amplitude of rapidly developing disturbances.

The initial testing of QNGM was carried out using NMC's limited area analysis and the LFM model's uniform horizontal grid. Predictions with QNGM are compared to those obtained with the LFM model in Section 7.

Several researchers have recently developed limited area models, e.g., Anthes and Warner (1978), Perkey (1976) and Kaplan *et al.* (1982). These models differ from each other and the QNGM in several aspects. For example, Perkey uses a somewhat detailed plume model to evaluate convective release of latent heat. A variation of Kuo's (1965) scheme is used in the QNGM. Anthes' (1977) scheme is used in the Anthes and Warner model. Convective release of latent heat has not yet been incorporated in Kaplan *et al.* (1982). A quasi-Lagrangian scheme is used for prediction in the QNGM. All other models employ Eulerian prediction schemes; however, the scheme employed is not the same in all models. A comparative study of predictions from these models in some test cases would be of interest but has not yet been attempted.

2. Predictive equations

The set of primitive equations with the quasi-static assumption on an appropriate Cartesian grid is used. The equations are as follows:

$$\frac{Du}{Dt} = A = \left[f + v\frac{\partial m}{\partial x} - u\frac{\partial m}{\partial y}\right]v - \dot{\sigma}\frac{\partial u}{\partial \sigma} - m\frac{\partial \phi}{\partial x} - mc_p\theta\frac{\partial \pi}{\partial x} + Fu\sigma, \quad (1)$$

$$\frac{Dv}{Dt} = B = -\left[f + v\frac{\partial m}{\partial x} - u\frac{\partial m}{\partial y}\right]u - \dot{\sigma}\frac{\partial v}{\partial \sigma} - m\frac{\partial \phi}{\partial y} - mc_p\theta\frac{\partial \pi}{\partial y} + F_{v\sigma}, \quad (2)$$

$$\frac{D\theta}{Dt} = C = -\dot{\sigma}\frac{\partial \theta}{\partial \sigma} + \frac{\theta}{c_pT}H + F_{\theta\sigma}, \quad (3)$$

$$\frac{Dq}{Dt} = D = -\dot{\sigma}\frac{\partial q}{\partial \sigma} + M + F_{q\sigma}, \quad (4)$$

$$\frac{D\ln p_{\text{sfc}}}{Dt} = E = -\nabla_\sigma \cdot \mathbf{V} - \frac{\partial \dot{\sigma}}{\partial \sigma}, \quad (5)$$

$$\frac{\partial \phi}{\partial \sigma} = -\frac{RT}{\sigma} = -c_p\theta\frac{\partial \pi}{\partial \sigma}. \quad (6)$$

Eq. (1) and (2) are the equations of motion in the x and y directions, respectively; Eq. (3) is a form of the first law of thermodynamics and (4) is a water vapor conservation equation. The equation of continuity (5) is used to predict the surface pressure p_{sfc}. Eq. (6) is the hydrostatic approximation.

The normal meteorological notation is used; u and v are the horizontal components of wind (**V**) in the x and y directions, respectively. The Coriolis parameter is f and m is the map factor. The other symbols which appear in the above equations are: T temperature, θ potential temperature, q mixing ratio, ϕ geopotential, c_p specific heat of air at constant pressure. H is the rate of heating and M is the change in mixing ratio due to convection. The nonconvective release of latent heat is evaluated at supersaturated grid points at the end of each time step. The last term in Eqs. (1)–(4) represent vertical exchanges by subgrid-scale processes excluding the diabatic effects mentioned above. D/Dt is the horizontal substantive derivative.

The Poisson equation is

$$\pi = \frac{T}{\theta} = \left(\frac{p}{100}\right)^\kappa$$

where p is pressure in *kpa* and $\kappa = 0.286$.

The vertical coordinate is $\sigma = p/p_{\text{sfc}}$ (Phillips, 1957) and $\dot{\sigma}$ is the vertical (σ) velocity.

The variables are not staggered in the horizontal. A caret above the variable denotes its value at a σ coordinate layer interface; a variable without the caret denotes its value in the layer; $\dot{\sigma}$ is calculated at the interfaces; u, v, ϕ, θ and q are evaluated in layers (see Fig. 1).

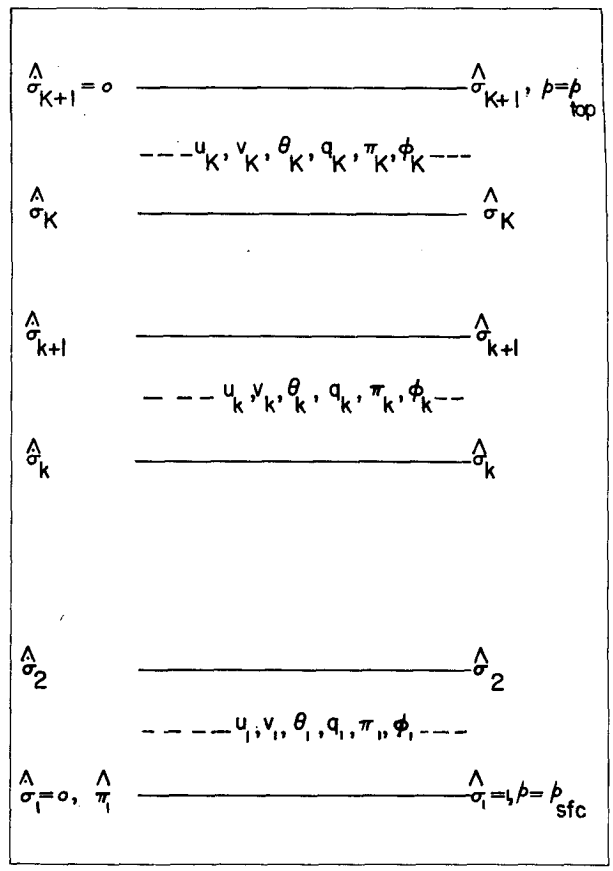

FIG. 1. Vertical staggering of variables.

The upper boundary of the model is at pressure $p_{\text{top}} = 0$. The boundary conditions are $\dot{\sigma} = 0$ at the top and the bottom of the model atmosphere.

3. Physical processes

Currently, only simple physical parameterization procedures are included in the model. The impact on forecasts from the use of more comprehensive parameterization procedures has not yet been fully investigated.

The bulk formulas used for computing sea to air sensible and latent heat transports, surface frictional effects, as well as the procedures used to evaluate convective and nonconvective latent heat release are now presented.

a. Vertical turbulent exchanges

The vertical eddy flux term in Eqs. (1)–(4) can be written as

$$F_{Q\sigma} = \frac{\partial \hat{\tau}_{Q\sigma}}{\partial \sigma},$$

where Q may be u, v, θ and q, respectively. The vertical

derivative in the above equation is evaluated using the second-order centered difference formula.

The surface frictional stress is given by

$$(\hat{\tau}_{u1}, \hat{\tau}_{v1}) = \frac{-gC_D}{RT_{\text{sfc}}}(u_1^2 + v_1^2)^{1/2}(u_1, v_1),$$

where R is the gas constant and C_D, the drag coefficient, is a function of wind speed. The temperature of air at the surface T_{sfc} is evaluated by extrapolating downward from the temperature of the first layer. The lapse rate of 0.0065 K m^{-1} is used.

The sensible and latent heat transfers from sea water to air, respectively, are

$$\hat{\tau}_{\theta 1} = \frac{gC_D}{RT_{\text{sfc}}}(u_1^2 + v_1^2)^{1/2}(T_{\text{sea}} - T_{\text{sfc}}),$$

$$\hat{\tau}_{q1} = \frac{gC_D}{RT_{\text{sfc}}}(u_1^2 + v_1^2)^{1/2}(q_{\text{sea}} - q_{\text{sfc}})$$

provided that the sea temperature $T_{\text{sea}} > T_{\text{sfc}}$. Note that $q_{\text{sea}} = q_s(T_{\text{sea}}, p_{\text{sfc}})$ where subscript s denotes the saturation value.

The turbulent stress terms above the surface interface are evaluated by the procedure given by Estoque and Bhumralkar (1969). The radiation physics and procedures to simulate the diurnal variations are now being tested but have not yet been incorporated in the model.

b. *Nonconvective release of latent heat*

The instantaneous isobaric condensation of water vapor is invoked if the predicted mixing ratio exceeds the saturation mixing ratio. Let (T_0, q_0, p) be the predicted temperature, mixing ratio and pressure, respectively, at a grid point when $q_0 > q_{s0}$. Here $q_{s0} = q_s(T_0, p)$. The adjusted temperature T_a and mixing ratio q_a are evaluated from

$$T_a = T_0 + \frac{q_0 - q_{s0}}{\frac{c_p}{L} + \frac{Lq_{s0}}{RT_0^2}}, \tag{7a}$$

$$q_a = q_0 - \frac{c_p}{L}(T_a - T_0), \tag{7b}$$

where L is the latent heat of vaporization. The value of q_a is very close to saturated value $q_s(T_a, p)$. Eq. (7) is derived by using the approximate relation $q_s = \epsilon e_s/p$ and a finite difference form of the Clausius-Clapeyron equation. Here ϵ is a constant and e_s the saturation vapor pressure. The derivation of (7) is given by McDonald (1963).

c. *Convective release of latent heat*

The parameterization of convective release of latent heat is patterned after the work of Kuo (1965). The model's convective cloud is given by the ascent through the lifting condensation level (LCL). The cloud parcel is allowed to originate from one of the three layers next to the ground. If the parcel originating from the lowest layer does not build a model cloud which is warmer than the environment in at least two adjacent layers[1] above the parcel's LCL, then the clouds are built with parcels originating in the next layer and so on.

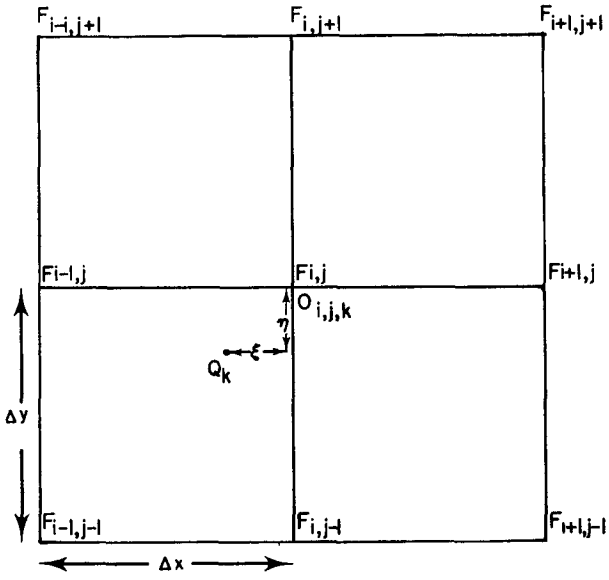

FIG. 2. Nine points for Lagrangian advection at any level k. A parcel originally at Q at time $t - \Delta t$ arrives at O at time t.

If a model cloud exists, then the rate of heating H [Eq. (3)] and the rate of increase of mixing ratio M [Eq. (4)] in a layer with pressure p due to convection are $HL(P)$ and $QL(P)$, respectively. Therefore,

$$HL(P) = c_p a[T_s(p) - T(p)],$$

$$QL(P) = a[q_s(p) - q(p)],$$

$$a = \frac{-\omega_B q_L}{\int_{pT}^{pB} \frac{c_p}{L}(T_s - T)dp + \int_{pT}^{pB}(q_s - q)dp}$$

provided that $\omega_B < 0$, $T_s > T$, and $q_s > q$, otherwise $HL(p) = 0$ and $QL(p) = 0$.

Here, p_B and p_T are the pressures at the interfaces k_1 and k_2, respectively (see footnote 1 for the definitions of k_1 and k_2). The temperature $T_s(p)$ and mixing ratio $q_s(p)$ are at pressure p in the model cloud, ω_B is the

[1] If k_1 is the lowest layer in which cloud is warmer than the environment, and k_2 the first layer above k_1 in which cloud is colder than the environment, then the convective clouds are assumed to exist in layers k_1 to $k_2 - 1$. The top of the clouds are also assumed not to reach above 100 mb. This gives an upper limit to k_2 in the model.

TABLE 1. NMC models used in intercomparison tests.

Model	Grid spacing (km)	Special initialization	Spatial finite differencing	Drag coefficient	Surface sensible heat flux	Surface latent heat flux
7L LFM (operational)	190.5	$\nabla_\sigma \cdot \mathbf{V} = 0$	fourth order (Deaven 1982)	varies with geography	over sea	over sea
7L LFM II (operational prior to June 1981)	127	$\nabla_\sigma \cdot \mathbf{V} = 0$	second order (Shuman and Hovermale 1968)	same as above	over sea	none
10L LFM	127	$\nabla_\sigma \cdot \mathbf{V} = 0$	same as above	same as above	over sea	none
10L QNGM	127	none	quasi-Lagrangian	varies with geography and wind speed	over sea	over sea

vertical p-velocity at the upper interface of layer L from which the parcel originates, and q_L is the mixing ratio in layer L. In order to conserve the mixing ratio, the amount $q_r = (0.5\omega_B q_L/\Delta p_r)$ is removed from each of the layers L and $L + 1$, where Δp_r is the thickness of layer r. Here, q_r is treated as a sink for mixing ratio and is included for layers L and $L + 1$ only in term M of Eq. (4).

4. Finite differencing procedures

A second-order quasi-Lagrangian scheme (Section 5) is used to integrate the model. It is therefore considered prudent to evaluate the derivatives which appear in Eqs. (1)–(5) using second-order centered difference formulas.

The evaluation of ϕ and π in layers is presently patterned after the energy conserving scheme of Arakawa and Mintz (1974). The application of this scheme to the NMC models is discussed by Brown (1974) and Phillips (1974).

The π in layers are given by

$$\pi_k = \frac{\hat{p}_k\hat{\pi}_k - \hat{p}_{k+1}\hat{\pi}_{k+1}}{(1+\kappa)(\hat{p}_k - \hat{p}_{k+1})}. \tag{8}$$

Note that (see Fig. 1)

$$\hat{p}_k = \hat{\sigma}_k\hat{p}_{\text{sfc}},$$
$$\hat{\pi}_k = \hat{\sigma}_k^{\kappa}\hat{\pi}_{\text{sfc}}.$$

Eq. (8) can be rewritten as

$$\pi_k = a_k\hat{\pi}_{\text{sfc}},$$

where

$$a_k = \frac{\hat{\sigma}_k^{\kappa+1} - \hat{\sigma}_{k+1}^{\kappa+1}}{(1+\kappa)(\hat{\sigma}_k - \hat{\sigma}_{k+1})}.$$

The ϕ's in layers 2 to K are given by

$$\phi_k = \phi_{k-1} - c_p\hat{\theta}_k(\pi_k - \pi_{k-1}), \tag{9}$$

where

$$\hat{\theta}_k = (\theta_k + \theta_{k-1})/2.$$

The ϕ of the first layer in the conserving scheme is given by

$$\phi_1 = \hat{\phi}_1 + \sum b_k\theta_k. \tag{10}$$

The sum in (10) is over all layers; the b_k are functions of $\hat{\pi}$ and $\hat{\sigma}$. In a test case the model was integrated first using (10) and subsequently using a simpler formula to evaluate ϕ_1, *viz.*,

$$\phi_1 = \hat{\phi}_1 + 0.5c_p\theta_1(\hat{\pi}_1 - \hat{\pi}_2). \tag{11}$$

The difference in the predicted fields at 48 h was small. Equation (11) is now used in the model to evaluate ϕ_1.

5. Quasi-Lagrangian advective scheme

A second-order quasi-Lagrangian scheme is used to integrate the model. The formulation of this scheme and numerical tests with the barotropic model are presented by Mathur (1984). The application of the scheme in the three-dimensional case with σ as the vertical coordinate is now presented. The difference between the quasi-Lagrangian schemes and Eulerian schemes is highlighted by comparing the prediction of surface pressure in the two schemes. The prediction

TABLE 2. Mean $S1$ scores from six test cases for mean sea-level pressure.

Forecast (h)	$S1$ score		
	7L LFM II	10L LFM	10L QNGM
12	37	36	35
24	47	46	46
36	55	56	53
48	57	59	58

TABLE 1. (*Continued*)

Model	Radiation		Precipitation		Special post processing
	Short-wave	Long-wave	Convective	Large scale	
7L LFM (operational)	yes	yes	convective adjustment	90–96% saturation criteria	Balanced height at 500 mb. Uses surface pressure tendency method.
7L LFM II (operational prior to June 1981)	yes	yes	same as above		same as above
10L LFM	yes	yes	same as above		same as above
10L QNGM	none	none	modified Kuo	100% saturation criteria	none

with the quasi-Lagrangian scheme is easier to interpret physically and the advective and forcing processes are evaluated with higher order accuracy than in the Eulerian scheme.

Equations (1)–(4) are integrated in the form

$$F_{i,j}^{n+1} = [(I - G)(I - H)W]_{i,j} + (R_{i,j}^{n} - 0.5R_{i,j}^{n-1})\Delta t, \quad (12)$$

where

$$(IW)_{i,j} = W_{i,j},$$

$$W_{i,j} = F_{i,j}^{n} + R_{i,j}^{n}\frac{\Delta t}{2}.$$

The superscript denotes the time level, and subscript i and j the horizontal indices in the x and y directions, respectively. $F_{i,j}^{n}$ is the value of one of the variables u, v, θ or q at any level k, and $DF/Dt = R$.

Here, G and H are second-order spatial finite difference operators in the x and y directions, respectively, i.e.,

$$G_{i,j} = \xi_{i,j}^{n}\delta_{i,j}^{x} - (\xi_{i,j}^{n})^2\delta_{i,j}^{2x},$$

$$H_{i,j} = \eta_{i,j}^{n}\delta_{i,j}^{y} - (\eta_{i,j}^{n})^2\delta_{i,j}^{2y},$$

where $\delta_{i,j}^{s}(F)$ and $\delta_{i,j}^{2s}(F)$ are the second-order, centered difference approximations to the first and second derivative of F with respect to s (i.e., x or y).

TABLE 3. Mean $S1$ scores from six test cases for height of 500 mb surface.

Forecast (h)	$S1$ score		
	7L LFM II	10L LFM	10L QNGM
12	30	28	27
24	34	35	33
36	36	38	35
48	41	42	40

The terms $\xi_{i,j}$ and $\eta_{i,j}$ are evaluated from

$$\xi_{i,j}^{n} = [(I - G')(I - H')X]_{i,j}, \quad (13)$$

$$\eta_{i,j}^{n} = [(I - G')(I - H')Y]_{i,j}, \quad (14)$$

where

$$X_{i,j} = u_{i,j}^{n}\Delta t + A_{i,j}^{n}\frac{\Delta t^2}{2},$$

$$Y_{i,j} = v_{i,j}^{n}\Delta t + B_{i,j}^{n}\frac{\Delta t^2}{2},$$

$$G'_{i,j} = X_{i,j}\delta_{i,j}^{x} - X_{i,j}^2\delta_{i,j}^{2x},$$

$$H'_{i,j} = Y_{i,j}\delta_{i,j}^{y} - Y_{i,j}^2\delta_{i,j}^{2y}.$$

Equation (5) is used to predict the surface pressure and also to evaluate $\dot{\sigma}_{n+1}$. Let $P = \ln p_{\text{sfc}}$, then at each level we have

$$P_{i,j}^{n+1} = [(I - G)(I - H)Z]_{i,j} + E_{i,j}^{n+1}\frac{\Delta t}{2}, \quad (15)$$

where

$$Z_{i,j} = P_{i,j}^{n} + E_{i,j}^{n}\frac{\Delta t}{2}. \quad (16)$$

Summation of (15) over all layers gives

$$P_{i,j}^{n+1} = \sum_{k=1}^{K}\Delta\sigma_k\left\{[(I - G)(I - H)Z]_{i,j} - (\nabla_\sigma\cdot\mathbf{V})_{i,j}^{n+1}\frac{\Delta t}{2}\right\}. \quad (17)$$

The sum involving $\dot{\sigma}^{n+1}$ vanishes because $\dot{\sigma} = 0$ at the top and bottom of the model atmosphere.

The variables u, v, θ and q are first predicted from Eq. (12), $(\nabla_\sigma\cdot\mathbf{V})_{i,j}^{n+1}$ is then evaluated from these predicted values. After $P_{i,j}^{n+1}$ is evaluated from (17),

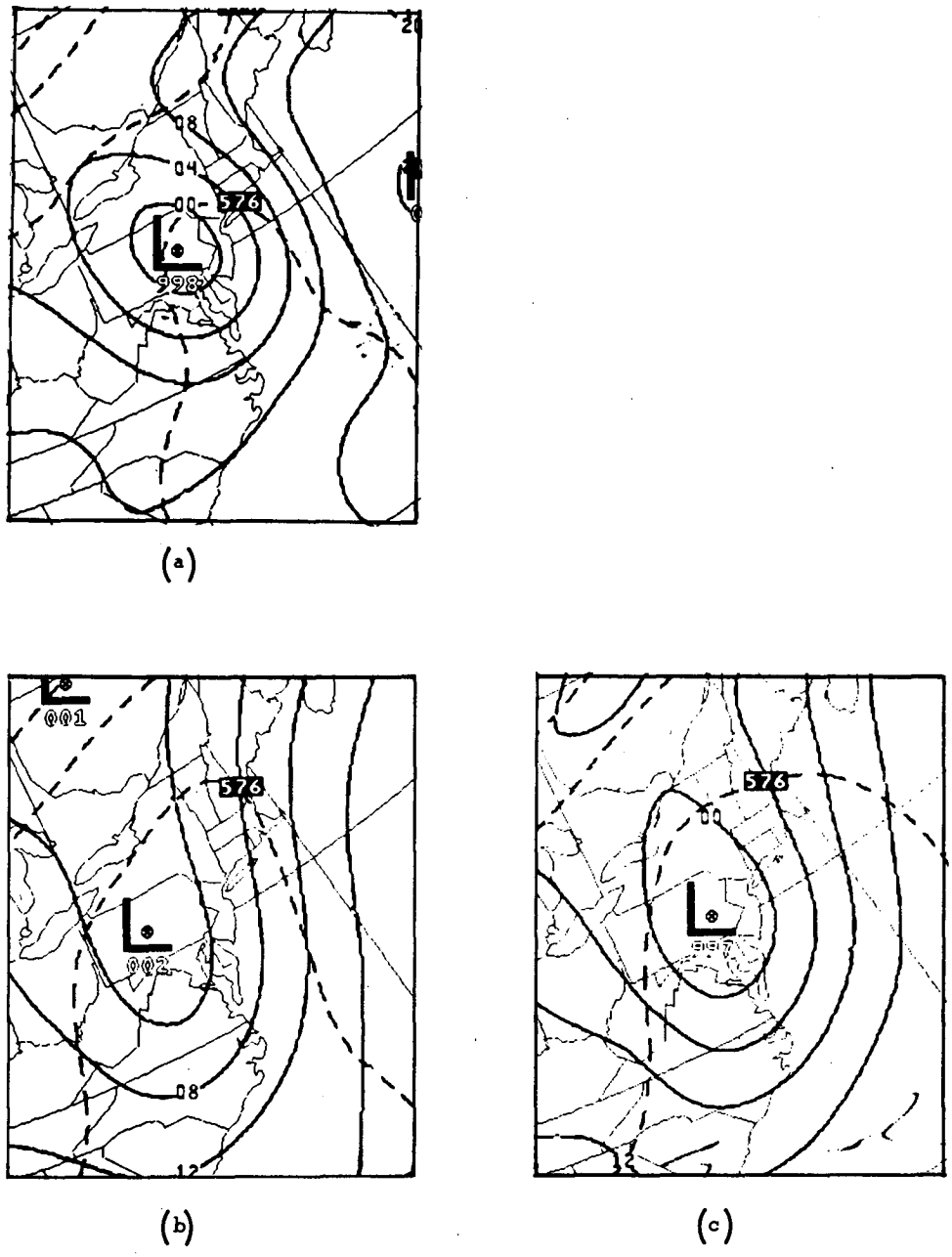

FIG. 3. The mean sea-level pressure (solid lines) and 1000–500 mb thickness (dashed lines) analyses valid at 1200 GMT 6 September 1979: (a) observed, (b) 24 h forecast from 10L LFM and (c) 24 h forecast from 10L QNGM. Isobars are drawn at intervals of 4 mb and thickness lines at intervals of 60 m.

$\overset{*}{\sigma}{}^{n+1}_{i,j,k}$ can be evaluated by integrating Eq. (15) for each layer k, starting from the top most layer K.

The differences between the quasi-Lagrangian and Eulerian prediction schemes are now briefly presented. We consider the prediction of surface pressure in the quasi-Lagrangian scheme; $\xi^n_{i,j}$ and $\eta^n_{i,j}$ define the location of a parcel Q_k at level k that arrives at the grid point $O_{i,j}$ after time Δt (Fig. 2)[2]. The operation $(I - G)(I - H)$ on F gives a second-order accurate, interpolated value of F at the point Q_k.

Since, in the baroclinic case, the wind and its ac-

[2] Computational stability of the quasi-Lagrangian scheme is discussed by Mathur (1970). The stability criteria are $\xi_{i,j} < \Delta x$ and $\eta_{i,j} < \Delta y$; Δx and Δy are the grid spacing.

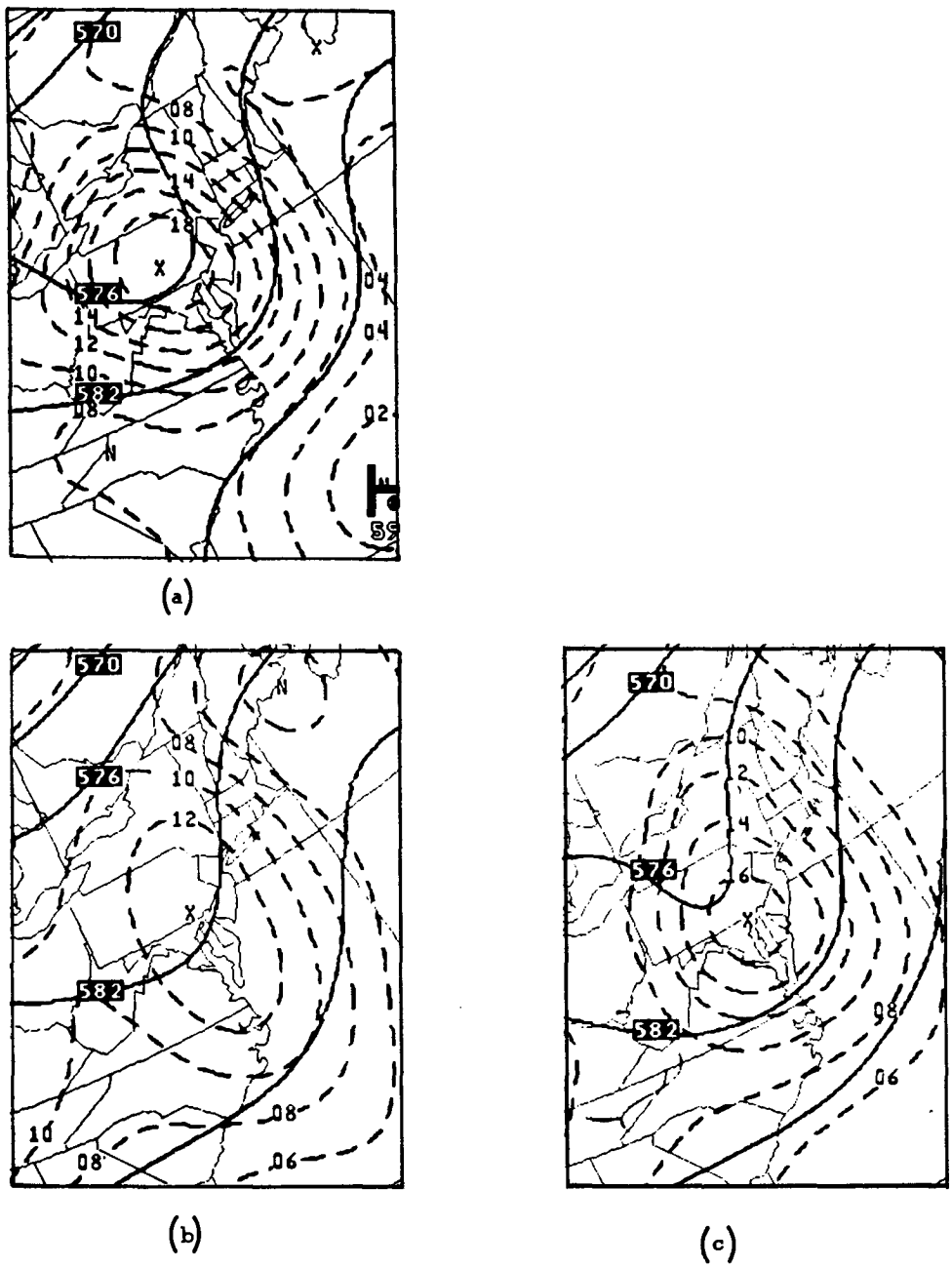

FIG. 4. The height (solid lines) and absolute vorticity (dashed lines) analysis at 500 mb valid 1200 GMT 6 September 1979: (a) observed, (b) 24 h forecast from 10L LFM, and (c) 24 h forecast from 10L QNGM. Height contours are drawn at intervals of 60 m and vorticity contours at intervals of 2×10^{-5} s^{-1}.

celeration vary in the vertical, the parcel Q_L at level L that arrives at the grid point $O_{i,j,L}$ in the interval of time Δt does not originate vertically above the parcel Q_m at another level m that arrives at the grid point $O_{i,j,m}$ (which is vertically above $O_{i,j,L}$) during the same interval of time. Here, the third subscript denotes the level. Therefore, when (16) is substituted in (17), we find that the sum S (given below) involving $\dot{\sigma}^n$ does not vanish in the equation for the prediction of surface pressure. Thus,

$$S = \sum_{k=1}^{K} \Delta\sigma_k \left[(I - G)(I - H) \frac{\partial \dot{\sigma}^n}{\partial \sigma} \right]_{i,j} \frac{\Delta t}{2}.$$

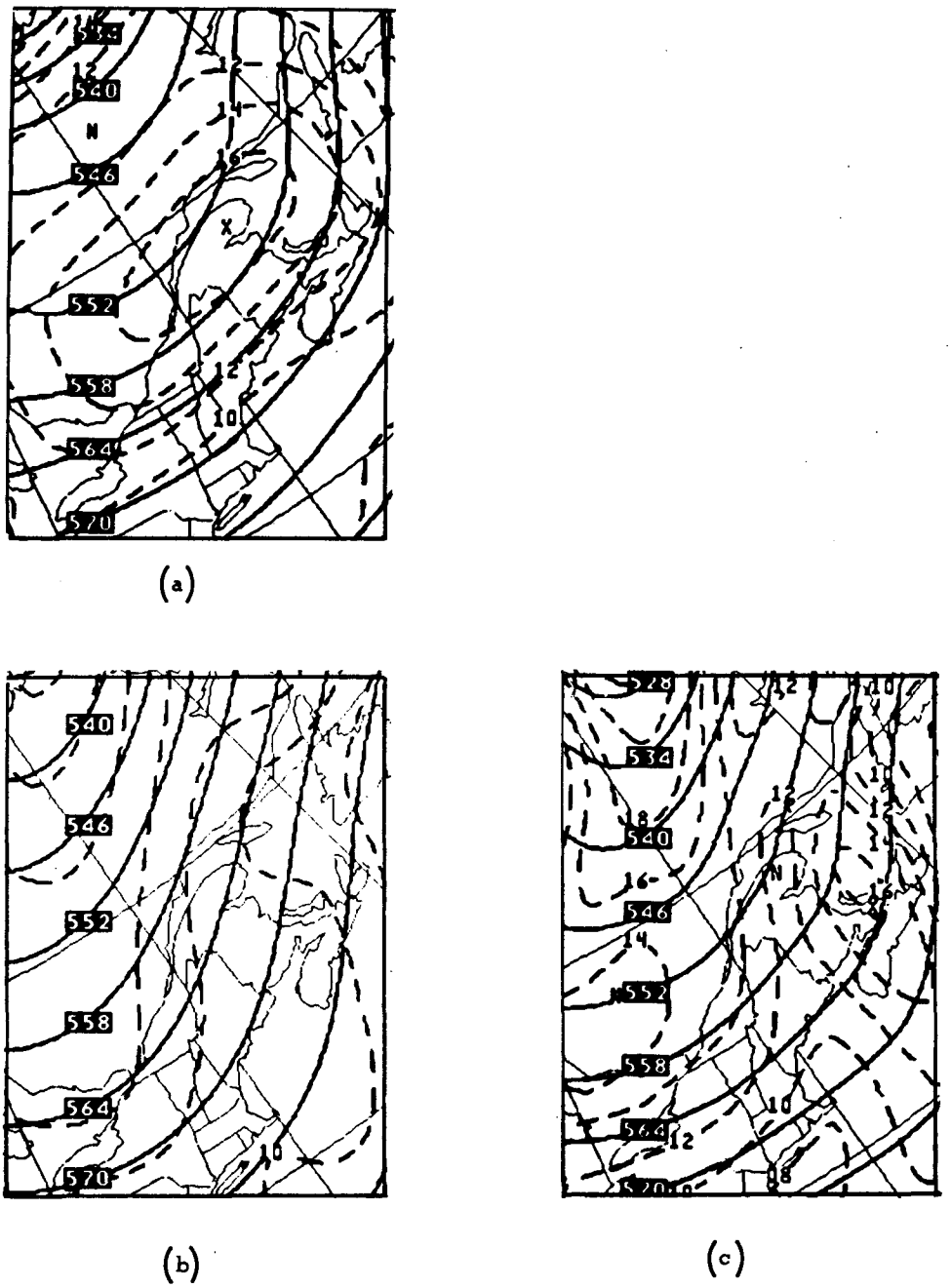

FIG. 5. The height (solid lines) and absolute vorticity (dashed lines) analysis at 500 mb valid 1200 GMT 7 September 1979: (a) observed, (b) 48 h forecast from 10L LFM, and (c) 48 h forecast from 10L QNGM. Units as in Fig. 4.

Equation (5) or some equivalent form of it is also included in models which are developed in Eulerian framework and use σ as the vertical coordinate (e.g., see Shuman and Hovermale, 1968). No term involving $\dot{\sigma}$ appears in the finite difference equation that is derived from (5) for the prediction of surface pressure in these models. This is because the accelerations are assumed to remain unchanged over the time step Δt in the Eulerian models. The change in accelerations during time step Δt is taken into account in the quasi-Lagrangian schemes (see Mathur, 1984). In order to demonstrate the above here, we rewrite (15) as

$$P_{i,j}^{n+1} = PQ^n + \frac{1}{2}(EQ^n + E_{i,j}^{n+1})\Delta t,$$

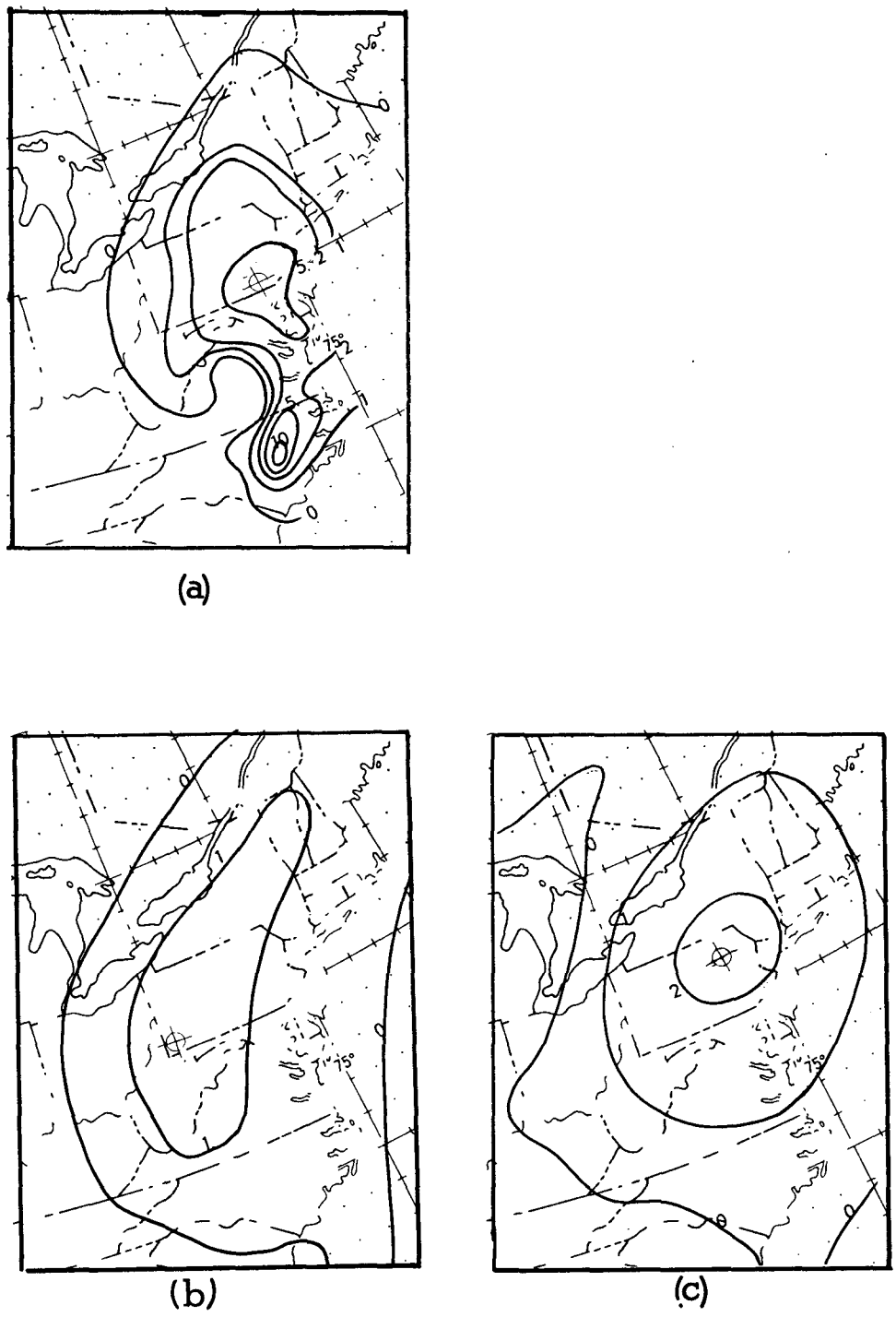

FIG. 6. 12 h precipitation amounts ending 1200 GMT 6 September: (a) observed, (b) 24 h forecast from 10L LFM, and (c) 24 h forecast from 10L QNGM. Units: cm.

where PQ^n and EQ^n are interpolated values of P^n and E^n at Q_k. The terms in parentheses represent the mean acceleration over the trajectory traced by the parcel during the time between $n\Delta t$ and $(n + 1)\Delta t$.

6. Initialization

The input to QNGM is currently derived from the LFM operational analyses. The input consists of u, v,

ϕ, θ and q at 12 standard pressure levels between 1000 and 50 mb and five map-related fixed variables. The five variables are the drag coefficient, the terrain height, the sea surface temperature, the map factor and the Coriolis parameter. Some other fixed variables like snow cover, albedo, etc., will be needed when radiation and other physical effects are incorporated in the model.

The procedures to compute the surface pressure, $\hat{\phi}$ at the interfaces $k = 2$, K, and (u, v) in layers $k = 2$, K are similar to those used in the operational LFM (see Gerrity, 1977). If the pressure at the interface (layer) k is less than 50 mb, then $\hat{\phi}(u, v)$ at k are obtained by an extrapolation procedure. The values of $\phi(u, v)$ at 70 and 50 mb are used in this extrapolation with $\ln p$ taken as the vertical coordinate.

The potential temperature in layers 1 to $K - 1$ are obtained from $\hat{\phi}$ with the use of the hydrostatic relation. The temperature θ in layer K is evaluated by an extrapolation procedure. First, $\hat{\theta}$ at interface K is obtained by interpolation, if $p_K > 50$ mb, and by extrapolation if $p_K < 50$ mb. The following condition is then imposed:

$$\theta_K = 2\hat{\theta}_K - \theta_{K-1}.$$

This procedure gives a reasonable initial mean value of θ in the uppermost layer.

7. Numerical results

The 10-layer (10L) QNGM has been integrated over LFM domain in several test cases. The numerical results from QNGM are compared with those obtained from LFM models. A comparison of QNGM with several versions of LFM used in this study is presented in Table 1. All models cover the same horizontal area and use polar stereographic map coordinates. The initial state in all models is obtained from the same operational analysis and the lateral boundary conditions from the same earlier run of the large-scale operational model.

A time step of 240 s is used in the QNGM. The 10L LFM uses a time averaging operator on pressure gradient in the equation of motion (see Brown and Campana, 1978) that allows LFM to use a time step of 400 s. The CPU time required by QNGM to produce a 48 h forecast is, however, the same as required by 10L LFM.

Immediately after the QNGM was developed in 1981, the predictions from the 10L QNGM, 7L LFM II and 10L LFM were compared in detail. The six test cases included various severe weather phenomena, *viz,* two summer cases of heavy precipitation over the eastern United States, the movement of tropical storm David, a development of severe winter storm over Ohio, an early snow storm over the Rockies, and a development of intense maximum in vorticity in the middle troposphere. The forecast skill of the three models was judged subjectively in the above six cases.

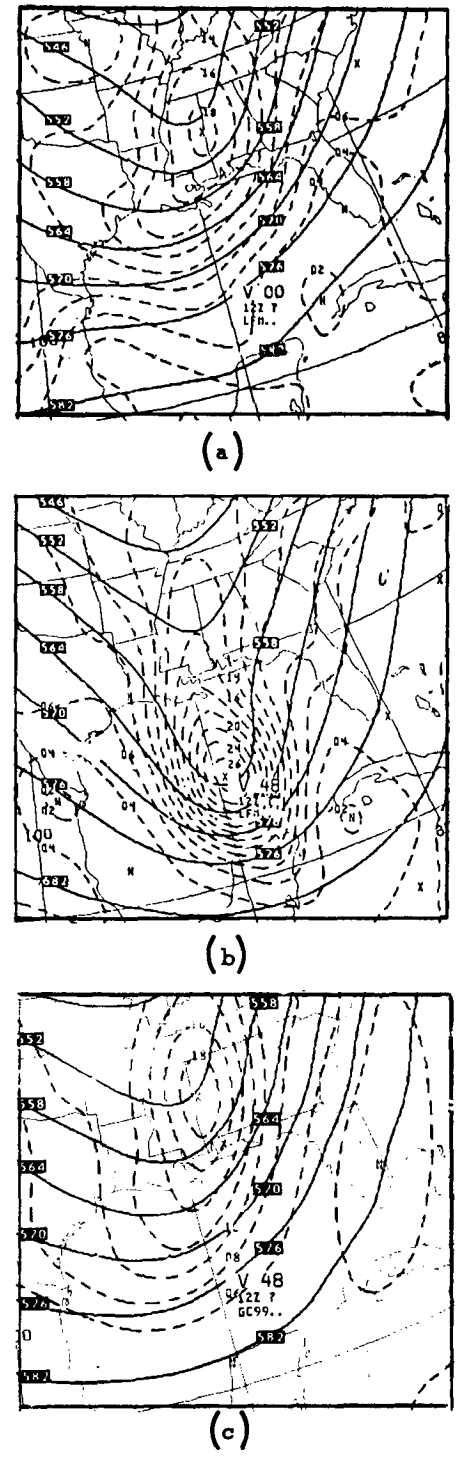

FIG. 7. The height (solid lines) and absolute vorticity (dashed lines) analysis at 500 mb valid 1200 GMT 7 March 1982: (a) observed, (b) 48 h forecast from 7L LFM, and (c) 48 h forecast from 10L QNGM. Units as in Fig. 4.

The QNGM was found to be either comparable to or better than both LFM models. For the statistical verification of the forecasts the mean $S1$ scores were com-

pared. The $S1$ score is defined (Teweles and Wobus, 1954) as

$$S1 = 100 \frac{\sum |e_g|}{\sum |G_L|},$$

where e_g is the error in the forecast pressure difference and G_L is the observed or forecast pressure difference between stations, whichever is largest. A maximum of 110 stations over United States were used. The mean $S1$ scores for mean sea-level pressure and the height of 500 mb surface are presented in Tables 2 and 3, respectively. The $S1$ scores from the QNGM are somewhat better than those obtained from the LFM models.

Contour analyses of predicted fields from QNGM and either 10L LFM or 7L LFM are now presented in two cases. The first case (Tropical Storm David) is one from the above six test cases. The second case, presented below, has been studied extensively at NMC because a large erroneous southward displacement of maximum in absolute vorticity ($\zeta_{a\max}$) was predicted by the operational LFM.

a. Case 1: Tropical Storm David 1979

Tropical Storm David was located over South Carolina (central pressure at 995 mb) at 1200 GMT, 5 September 1979. The storm moved north northeastward with little change in its intensity and was positioned over eastern Pennsylvania at 1200 GMT 6 September (Fig. 3a). An open low with a lowest pressure of 1002 mb, near the observed center of David, is predicted by the 10L LFM (Fig. 3b). An open low with pressure of 1008 mb, near the observed center, was predicted by 7L LFM. A more intense low, with a central pressure of 997 mb, is predicted by the 10L QNGM (Fig. 3c).

The storm center was located near 48°N, 62°W (central pressure at 986 mb) at 1200 GMT 7 September. The 48 h QNGM forecast valid at that time showed an elongated low pressure area with two centers (both with a pressure of 984 mb) at 49°N, 62°W and 53°N, 58°W. The 10L LFM also predicted an elongated low pressure area with two centers: 1) 992 mb at 54°N, 55°W and 2) 995 mb at 48°N, 63°W. A low pressure center (998 mb) was located at 51°N, 60°W in the 7L LFM forecast.

A $\zeta_{a\max}$ of 18 units (10^{-5} s^{-1}) was located over the surface position of David at 1200 GMT 6 September (Fig. 4a). The predicted $\zeta_{a\max}$ is 12 units in the 10L LFM (Fig. 4b), 14 units in the 7L LFM, and 16 units in the 10L QNGM (Fig. 4c). The superior performance of QNGM over the LFM is further demonstrated in the 48 h predictions. The $\zeta_{a\max}$ of 16 units is located in QNGM (Fig. 5c) near the area of observed $\zeta_{a\max}$ of 16 units (see Fig. 5a). A closed maximum in absolute vorticity is not predicted in either the 10L LFM (Fig. 5b) or the 7L LFM.

The observed 12 h rainfall amounts ending 1200 GMT 6 September are shown in Fig. 6a. A large area with amounts exceeding 5 cm extends from Virginia to Pennsylvania. The predicted precipitation amounts are somewhat better in the 10L QNGM (Fig. 6c) than the 10L LFM (Fig. 6b). The amounts predicted by the 7L LFM were smaller.

In summary, the precipitation and the intensity of Tropical Storm David at the surface and the middle troposphere were predicted better by the 10L QNGM than by the 10L LFM or 7L LFM models.

b. Case 2: Movement of midtropospheric vorticity maximum (5 March 1982)

Recently, it has been noticed that the operational 7L LFM model often predicts erroneously large southward displacement of centers of $\zeta_{a\max}$ over the southeast United States. As an illustration, the 48 h prediction at 500 mb from 1200 GMT 5 March 1982 is shown in Fig. 7b. The $\zeta_{a\max}$ which is centered in the Gulf of Mexico is located over the Mississippi–Alabama border in the verifying analysis (Fig. 7a). The $\zeta_{a\max}$ was located over northwest Mexico at the initial time. Dr. J. Gerrity (personal communication, 1983) found that similar erroneous predictions are made by the 10L and 7L LFM using LFM II grid spacing. The above error was not present in the predictions with NMC's spectral (global) model. The initial state in the spectral model is obtained from the NMC's Hough analysis. The above LFM models were also integrated with the initial state derived from the Hough analysis. The erroneous displacement of $\zeta_{a\max}$ was also present in these predictions. The error in the predictions with the LFM is therefore not related to errors in initial analysis or to the lack of horizontal and vertical resolution.

The 10L QNGM was integrated using the operational LFM analysis. The error in the location of $\zeta_{a\max}$ which occurs in LFM predictions was not present in QNGM forecast. The location and intensity of $\zeta_{a\max}$ at 48 h (Fig. 7c) agrees very well with the verifying analysis (Fig. 7a).

c. Related work

A test of the QNGM model using higher vertical resolution has been completed (Mathur, 1982). The intensity of the middle tropospheric circulation associated with Tropical Storm David was predicted better when the vertical resolution was increased from 10 to 15 or to 20 layers. Consequently, there was also an improvement in the prediction of the intensity of the surface disturbance and in the amounts of precipitation.

The nested grid version of the QNGM has been also tested. The fine mesh which has twice the resolution of the coarse mesh can be located anywhere inside the coarse mesh. For the test case (tropical storm David), the fine mesh with twice the resolution of the LFM II

grid covered most of the United States and adjoining Atlantic Ocean; ten layers were used. The intensity of the storm in the lower and middle troposphere and the precipitation amounts were predicted better in the nested model than in the model using uniform, LFM II grid spacing. The results of this comparison and procedures used to initialize the nested model will be presented in a separate report.[3]

8. Summary

A quasi-Lagrangian model was developed and tested. The prediction scheme formulated by Mathur (1984) is used. The variation of advecting velocity and of forcing of the dependent variables over the time step Δt is taken into account in this scheme. The motivation for developing the model was that the use of a high order accurate advective scheme would lead to an accurate prediction of intensity and movement of atmospheric circulations and of precipitation. Although the model is intended for use as an operational prediction model, it is also suitable for research work. The model can be integrated over any geographical area and with any desired resolution. Furthermore, the model is designed so that new physical parameterization procedures can easily be introduced in it.

A 10L version of the QNGM was integrated over the LFM domain in several test cases and the predictions from the QNGM were compared with predictions from the LFM models. The initial states in the QNGM and LFM models were derived from the same operational analysis, and lateral boundary conditions from the same run of an operational larger scale model. The parameterization of physical processes is somewhat different in the QNGM than in the LFM models (Table 1). The most significant difference is in the parameterization of convective rain. A Kuo-type parameterization scheme is used in the QNGM and a convective adjustment scheme in the LFM. Numerical results in a test case (Section 7b) showed that a characteristic error which is often observed in LFM forecasts, *viz*, a large erroneous southward displacement of $\zeta_{a\max}$ at 500 mb over the southeast United States, was not present in the QNGM forecast. The improved performance of the QNGM over the LFM is most likely related to the use of a higher order of accuracy in the advective scheme in QNGM compared to the scheme used in the LFM models. In the cases where the intensity of disturbance is predicted better in the QNGM, compared to that in the LFM models, e.g., intensity of Tropical Storm David (Section 7a), the somewhat better parameterization procedures used in the QNGM than the LFM would have also contributed in producing better forecasts.

We plan to include in the model both radiational effects and a more detailed boundary layer parameterization to simulate diurnal variations. We also plan to convert the code for efficient integration on vector-processor computers. The feasibility of using the model for operational prediction of mesoscale or synoptic-scale features will then be considered.

[3] These results were also presented at the WMO Regional Scientific Conference on Tropical Meteorology, 18–22 October 1982, Tsukuba, Japan.

REFERENCES

Anthes, R. A., 1977: A cumulus parameterization scheme utilizing a one-dimensional cloud model. *Mon. Wea. Rev.*, **105,** 270–286.

——, and T. T. Warner, 1978: Development of hydrodynamic models suitable for air pollution and other meteorological studies. *Mon. Wea. Rev.*, **106,** 1045–1078.

Arakawa, A., and Y. Mintz, 1974: The UCLA atmospheric circulation model. Dept. of Meteorology, University of California, Los Angeles, 320 pp.

Brown, J. A., 1974: On vertical differencing in the sigma system. NMC Office Note 92, 13 pp. [National Meteorological Center, NOAA, Washington, DC 20233.]

——, and K. A. Campana, 1978: An economical time-differencing system for numerical weather prediction. *J. Atmos. Sci.*, **106,** 1125–1136.

Deaven, D., 1982: More efficient LFM by applying fourth order operators. Tech. Proc. Bull., No. 300, Meteorological Services Division, NOAA, [National Meteorological Center], 9 pp.

Estoque, M. A., and C. M. Bhumralkar, 1969: Flow over a localized heat source. *Mon. Wea. Rev.*, **97,** 850–858.

Gerrity, J. G., 1977: The LFM Model 1976: A documentation. NOAA Tech. Memo. NWS NMC-60. 68 pp. [NTIS PB-279-419.]

Kaplan, M. L., J. W. Zack, V. C. Wong and J. J. Tuccillo, 1982: Initial results from a mesoscale atmospheric simulation system and comparisons with the AVE-SESAME I Data Set. *Mon. Wea. Rev.*, **110,** 1564–1590.

Kuo, H. L., 1965: On formation and intensification of tropical cyclones through latent heat release by cumulus convection. *J. Atmos. Sci.*, **22,** 40–63.

Mathur, M. B., 1970: A note on an improved quasi-Lagrangian advective scheme for primitive equations. *Mon. Wea. Rev.*, **98,** 214–219.

——, 1974: A multiple-grid primitive equation model to simulate the development of an asymmetric hurricane (Isbell, 1964). *J. Atmos. Sci.*, **31,** 371–393.

——, 1982: Further experimentations with quasi-Lagrangian prediction model: Effect of high vertical resolution. NMC Office Note 260, 10 pp. [National Meteorological Center].

——, 1984: On the formulation of quasi-Lagrangian prediction schemes for numerical weather prediction. (Submitted to *Mon. Wea. Rev.*)

McDonald, J. E., 1963: The saturation adjustment in numerical modelling of fog. *J. Atmos. Sci.*, **20,** 476–478.

Perkey, D. J., 1976: A description and preliminary results from a fine-mesh model for forecasting quantitative precipitation. *Mon. Wea. Rev.*, **104,** 1513–1526.

Phillips, N. A., 1957: A coordinate system having some special advantages for numerical forecasting. *J. Meteor.*, **14,** 184–185.

——, 1974: Application of Arakawa's energy-conserving scheme to operational numerical weather prediction. NMC Office Note No. 104, 40 pp.

Shuman, F., and J. B. Hovermale, 1968: An operational six-layer primitive equation model. *J. Appl. Meteor.*, **7,** 525–547.

Teweles, S., and H. B. Wobus, 1954: Verification of prognostic charts. *Bull. Amer. Meteor. Soc.*, **35,** 455–463.